Axial Super-Resolution Ultrasound Imaging With Quasi-Monopolar Pulses From a Dual-Frequency Transducer

Yiqi Cai, Mengzhi Fan, Pengfei Sun, Lijun Xu, *Fellow, IEEE*, and Jianguo Ma, *Member, IEEE*

***Abstract*— In biomedical ultrasound imaging, the axial resolution is determined by the pulse length, which reaches the bottleneck for the existing piezoelectric materials. The resonance of piezoelectric materials in conventional ultrasound transducers causes relatively long pulses with multiple wavelengths, which cannot be effectively shortened for decades. The waveform with practically the shortest pulse length is a monopolar half-cycle sinusoidal wave, which is beyond the capability of traditional piezoelectric transducers. Here, we propose a method for generating quasi-monopolar ultrasound pulses by the superposition of two ultrasound signals from a stack-layer dual-frequency ultrasound transducer. In this article, we designed and fabricated a 1 + 3 MHz stack-layer dual-frequency ultrasound transducer, and validated the generation of the quasi-monopolar pulse by specific excitation of each piezoelectric layer. Imaging with the quasi-monopolar pulses on copper wire phantoms demonstrated a pulse length of 0.17λ (85.5 ns referring to 2 MHz), which generates images with superb axial resolution and clearly differentiates the phantom wires separated with 1 mm. This design provides a practical approach for general-purpose super-resolution ultrasound imaging without a contrast agent.**

***Index Terms*— Dual-frequency ultrasound transducer, monopolar ultrasound pulse, super-resolution, superposition, ultrasound imaging.**

I. Introduction

IN BIOMEDICAL imaging, the promotion of resolutions in a given depth is an eternal goal [1], [2], which drives modern medical imaging modalities to cutting-edge performances. For ultrasound imaging, the bottleneck of axial resolution is the inability to further decrease the pulse length at a given center frequency. Because of relatively strong resonance, the pulse length emitted by traditional piezoelectric ultrasound transducers is typically at least 1.5 cycles [3], [4], [5], [6], which defines the limit of traditional ultrasound imaging. Super-resolution of vasculature by tracking microbubbles overcomes the limit and reveals extremely fine structures deep inside mouse brains [7]. However, the super-resolution of normal tissues without injection of contrast agent remains an unmet theoretical and technical challenge. Overcoming this challenge requires the excitation, reception, and processing of very short pulses.

Monopolar ultrasound pulses are the shortest waveform practically achievable for a finite bandwidth, which potentially enables super-resolution in brightness mode (B-mode) ultrasound imaging, harmonic imaging, and spectrum analysis for cutting-edge biomedical imaging. In general ultrasound imaging, decreasing the time duration of the pulses indicates a promotion in spatial resolution due to the capability to differentiate successive echoes from adjacent scatters [8], [9], [10], [11], [12]. Increasing the center frequency, as one approach, is not ideal because of its sacrifice on penetration depth [13], [14], [15], [16], [17]. The optimal approach is to decrease the number of cycles in each pulse, which decreases the pulse length while maintaining the center frequency. The monopolar pulse, e.g., a half cycle of a sinusoidal wave, yields the highest resolution images theoretically without super-resolution techniques. In ultrasound harmonic imaging, a negative monopolar pulse is ideal to generate nonlinear harmonic responses because it is almost free of noises at positions other than the peak negative pressure [18], [19], [20]. Meanwhile, a monopolar pulse is associated with a broad bandwidth, e.g., the −6 dB fractional bandwidth approaching 200%, which provides rich information that is valuable for tissue characterization. Therefore, the generation of monopolar pulses is one of the ultimate goals for ultrasound transducer design.

However, the generation of absolute monopolar pulses is beyond the capability of traditional piezoelectric ultrasound transducers. Because of the high acoustic impedance and high-quality factor, vibration at piezoelectric layers dissipates relatively slowly, elongating the pulse length and decreasing the bandwidth [21], [22]. Matching layers are included to promote the transmission efficiency from the piezoelectric material to bodies [23], [24], [25]. Nevertheless, the matching layers are ideal at the designed frequency only, which is incapable of transmission of broadband monopolar signals. The impedance of backing layers is typically lower than the piezoelectric material, which does not dissipate the excessive vibrations instantly. Because of these inherent limitations, the shortest pulses generated by traditional piezoelectric ultrasound transducers are about 1.5 cycles, which corresponds to a −6 dB fractional bandwidth of ∼70% [4], [5], [6].

Manuscript received 16 October 2022; revised 1 December 2022; accepted 16 December 2022. Date of publication 9 January 2023; date of current version 12 January 2023. This work was supported in part by the National Science Foundation of China under Grant 61901021 and Grant 82127804, and in part by the Capital's Funds for Health Improvement and Research under Grant 2022-4-1105. The Associate Editor coordinating the review process was Dr. Alvaro Hernandez. *(Corresponding author: Jianguo Ma.)*

Yiqi Cai, Mengzhi Fan, Lijun Xu, and Jianguo Ma are with the School of Instrumentation and Optoelectronics Engineering, Beihang University, Beijing 100191, China (e-mail: majianguo@buaa.edu.cn).

Pengfei Sun is with the Department of Ultrasound, Beijing Friendship Hospital, Capital Medical University, Beijing 100050, China.

Digital Object Identifier 10.1109/TIM.2023.3234032

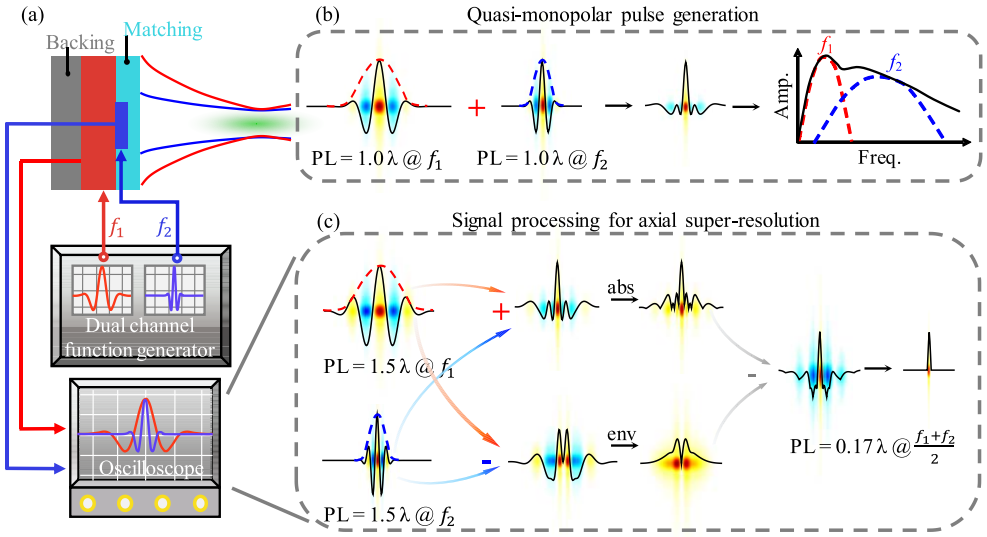

Fig. 1. (a) Schematic diagram of the dual-frequency ultrasonic transducer used to generate quasi-monopole ultrasonic pulses. (b) Superposition process and spectrum of quasi-monopolar ultrasonic pulses, the bandwidth of the dual-frequency signal is about 90%. (c) Signal processing of super-resolution ultrasound images. The pulse-echo bandwidth of the dual-frequency signal is set to 70%.

Enormous efforts have been devoted to decreasing the number of cycles in each pulse. First, piezoelectric 1–3 composite has been developed to lower the acoustic impedance and the quality factor, which decreases the pulse length to about 1.1 cycles and promotes the −6 dB fractional bandwidth to ∼90% [26], [27]. Second, the capacitive micro-machined ultrasound transducer (CMUT) and piezoelectric micro-machined ultrasonic transducers (PMUTs) has been demonstrated the generation of sub-wavelength pulses and a bandwidth of 120% [28], [29], [30], [31], [32], which holds great potential for high-performance ultrasound transducers in the future. Moreover, a variety of cutting-edge methods have been proposed, such as the deconvolution neural network-based method to achieve the nondestructive testing of super-resolution imaging [33], and new excitation signals to extend the response signal spectrum method [34]. These approaches have made great breakthroughs compared to traditional ultrasound transducers. Nevertheless, their performances are still far from monopolar pulses.

Another alternative for the generation of monopolar ultrasound pulses is the superposition of multiple wavelets with different center frequencies [35]. According to wavelet transform theory, a monopolar pulse is decomposed into a series of wavelets with a relatively narrower bandwidth. Generation of each wavelet is achievable by an ultrasound transducer. Therefore, monopolar ultrasound pulses are generated by the superposition of these wavelets from 23 transducers with five frequencies and a specific time delay. The pulse length is nearly half-cycle and the −6 dB fractional bandwidth is more than 150%, which outperforms all the other approaches. The constraints for this method include the complex system setup and the inability of beam steering because monopolar pulse happens only at the co-focal point of all the 23 transducers. It is unrealistic to extend this setup to linear or phased arrays for biomedical imaging. We previously proposed a mechanism for generating quasi-monopolar ultrasound pulses by a stack-layer dual-frequency ultrasound transducer [36], [37]. This indicates the potential of ultrasound imaging with high axial resolution.

In this article, we propose a super-resolution method in the axial direction by quasi-monopolar ultrasound pulses for biomedical applications. Following the previous work, the quasi-monopolar pulses are generated by the superposition of two frequencies from a stack-layer dual-frequency ultrasound transducer. The frequency and amplitude ratio of the two pulses are optimized to obtain quasi-monopolar ultrasound pulses with high peak-to-peak ratios. Echoes of the quasi-monopolar pulses are received by both elements of the dual-frequency transducer. Furthermore, we developed customized signal processing methods to maximize the performance of the quasi-monopolar ultrasound pulses in biomedical imaging, and obtained ultrasound images with unprecedently fine structures approaching the actual width of the tested phantom wires.

II. Methods

A. General Strategy

The overall strategy of quasi-monopolar excitation and reception is to cover its ultra-broad bandwidth with a corresponding dual-frequency transducer. According to wavelet transformation in linear acoustics, a short monopolar impulse is decomposable into a series of wavelets, and vice versa. However, an absolute monopolar signal, e.g., the impulse waveform with a delta function is impossible to realize due to the infinitely broad bandwidth. The realistic process is to decompose a quasi-monopolar pulse into a finite number of wavelets with a few center frequencies, and reconstruct the quasi-monopolar pulses from them (Fig. 1). Considering the difficulties in fabricating ultrasound transducers with three or more center frequencies, this pioneering research transmits

and receives the quasi-monopolar with two center frequencies from a stack-layer dual-frequency transducer. Each of the sub-band signals is considered a Morlet wavelet with a fractional bandwidth of 70%, which is achievable by the piezoelectric ultrasound transducer. The overall process consists of the transmission and reception of the dual-frequency waves, the superposition to generate quasi-monopolar pulses, and the digital signal processing to generate short pulses for imaging (Fig. 1).

A dual-frequency ultrasound system transmits the two wavelets to reconstruct the quasi-monopolar pulses. A dual-channel function generator sends electrical pulses at given center frequencies to a dual-frequency ultrasound transducer [Fig. 1(a)]. The signal phase of each channel is tuned to maximize the amplitude of the acoustic output at one peak. The relative time delay of the two excitations is adjusted to coincide with the peaks of the two frequencies. Every point inside the main beam along the axial axis undergoes the excitation of both frequencies. Therefore, the superposition of the two frequencies generates a quasi-monopolar pulse with a very short time duration [Fig. 1(b)].

Processing of the dual-frequency signals yields short pulses for axial super-resolution imaging [Fig. 1(c)]. First, the two signals are synchronized according to the relative position of the two piezoelectric layers. The peaks of them are automatically aligned with each other. Second, the two signals are processed in two separate ways to generate the waveform with the peak and the envelope without the peak. Because of the in-phase superposition at the peak, the sum of the dual-frequency signals yields a high amplitude at the peak, and a low amplitude at other positions [upper route in Fig. 1(c)]. The absolute value of the summed signal reverses the peak in case it is negative. In the other route, subtraction between the dual-frequency signals leaves the whole signal except the peak, and the envelope is high around the wavelet except for the position of the peak [lower route in Fig. 1(c)]. Subtraction of the envelope from the summed-and-absolute signal leads to a waveform with high amplitude at the peak and non-positive values at other positions [right in Fig. 1(c)]. Neglecting the negative values, the positive portion of the waveform demonstrates a precise distance of the imaging target, indicating an axial super-resolution in ultrasound imaging.

The optimization goal of this research is to maximize the peak while suppressing the noises around it. Here, we quantitatively define the amplitude ratio of the quasi-monopolar acoustic pulse [Fig. 1(b)] between the peak pressure (P_P) and the pressure of the residual waveforms (P_R)

$$\eta = \frac{\text{peak pressure (absolute value)}}{\text{residual pressure (peak} - \text{to} - \text{peak)}}.$$

Maximizing the ratio η leads to axial super-resolution imaging with a high signal-to-noise ratio (SNR). In the optimization, the amplitude and the center frequency of the low-frequency wavelet are set as the reference, which acts as fundamentals of the quasi-monopolar pulse. Pulses with other low frequencies or amplitudes are linear scaling in the time or amplitude domain. Considering the availability of frequency combinations in a dual-frequency transducer, the frequency ratio (high frequency to low frequency) ranges from 2:1 to 4.5:1. Moreover, the amplitude of the two wavelets has to be comparable to make a contribution to the superposition. Therefore, the amplitude ratio (high frequency to low frequency) is evaluated within the ranges from 0.5:1 to 3.5:1.

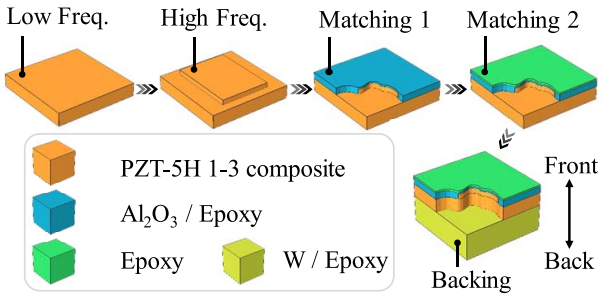

Fig. 2. Schematic diagram of the fabricating process.

B. Dual-Frequency Ultrasound Transducer

Generation of quasi-monopolar pulses requires the overlap of the two beams at the two frequencies, which is ideally achievable by a stack-layer dual-frequency ultrasound transducer [38], [39], [40]. In the transducer, a high-frequency element at 3 MHz center frequency is arranged in front of a low-frequency element at 1 MHz center frequency. As the two piezoelectric layers of the two frequencies share the aperture, each beam covers the field in front of the transducer. In the region shared by the two beams, the acoustic vibrations are the superposition of both beams, which enables the generation of the quasi-monopolar pulse.

The stack-layer dual-frequency transducer consists of two ultrasonic elements corresponding to the two frequencies (final configuration in Fig. 2). The active material of both elements is PZT-5H 1–3 composite for a relatively broad bandwidth. Considering the frequency-dependent loss and the vibration condition, the high-frequency element is set at the front (close to the load), while the low-frequency element is set at the back (close to the backing layer). The high-frequency element consists of double-matching layers for broadband transmission. The low-frequency piezoelectric layer is attached to the back of the high-frequency piezoelectric layer directly. All the layers in front of the low-frequency layer, including the double matching layers and the piezoelectric layers, act as the matching layers of the low-frequency element. Both elements share a heavy backing layer at the back of the low-frequency piezoelectric layer. Detailed material information is listed in Table I.

Prototypes are fabricated according to the design of the stack-layer dual-frequency ultrasound transducer (Fig. 2). The fabrication process starts with piezoelectric plates with chromium/gold (Cr/Au) electrodes coated on the surfaces. A 1–3 composite piezoelectric plate (low-frequency) with a gold-plated layer was fixed onto a glass plate using paraffin wax. The high-frequency 1–3 composite piezoelectric plate with Cr/Au electrodes is bonded directly to the low-frequency

TABLE I
MATERIAL PARAMETER

Parameters	PZT-5H 1-3 composite	The 1st matching	The 2nd matching	Backing
Longitudinal Velocity (m/s)	3220	2923	2556	1715
Density (kg/m^3)	4040	1865	1130	7914
Acoustic impedance (MRayl)	13.0	5.5	2.9	11.7
Thickness (μm)	533/1600	203	330	NA

Epoxy: EPO-TEK 301

element. As the first matching layer, the mixture of alumina (1 μm particle size) and epoxy (Epo-tek 301, Epoxy Technology Inc., Billerica, MA, USA) is cast on top of the piezoelectric layer and lap to the design thickness after cure. The epoxy resin, the second matching layer, is then cast on top of the first matching layer and lap to the design thickness after cure. After that, the sample is detached from the glass substrate, and the backing layer with a thickness of 20 mm is attached to the back surface of the low-frequency element. In each step of the fabrication process, part of the electrode is left uncovered for wire bonding. The transducer is finally housed in an aluminum tube with an inner diameter of 15 mm.

The finite element method (FEM) is used to simulate the quasi-monopolar pulses of the proposed transducer. In FEM, the material parameters and their thicknesses comply with the transducer designs demonstrated in Table I. To ensure the spatial accuracy of the simulation, the maximum frequency of the whole model is set to 5 MHz to cover both bands of the dual-frequency transducer, and the mesh size is within 0.2λ at this maximum frequency. For an accurate sampling in the time domain, the time interval for FEM simulation is 4 ns, which is 0.02 cycles of the maximum frequency. The time range for the simulation was 6 μs, which covers all the direct wave propagations in the model. Both low-frequency and high-frequency piezoelectric layers are stimulated by a tuned one-period sinusoidal wave.

C. Characterization of Acoustic Pulses

We verified the generation of quasi-monopolar ultrasound pulses by synchronized excitation of the dual-frequency elements with a specific delay time. Each element is excited by a single-cycle sinusoidal waveform, and both electrical excitations are generated by a dual-channel function generator (UTG2062B, Uni-Trend Technology Company, Ltd., Dongguan, Guangdong, China) to ensure the desired time delay. The phase of the excitation signal is manually tuned to compensate for the phase delay between the two elements from position variations and to ensure the coincidence of peaks between the two frequencies. The phase delay is transducer-dependent only, which does not need further tuning in the imaging process. All the parameters for the low-frequency element remained constant, whereas the parameters of the high-frequency element, i.e., the frequency and the amplitude, were adjusted to maximize the ratio between the peak pressure and the residual pressure (η). Transmission sensitivity, i.e., the pressure output at given electrical excitation, at each specific frequency was calibrated by a hydrophone (HGL-0200, Onda Corporation, Sunnyvale, CA, USA) to ensure the accuracy of each wavelet and the superposition output. All the waveforms were measured at 30 mm away from the transducer, which is twice the natural focal distance for both frequencies. The acoustic beam at this position is relatively strong and uniform so as to alleviate the errors from slight noises or deviations of the position in the measurement, and the 30 mm test distance is also a typical depth for medical applications. The acoustic waveform measured by the hydrophone is amplified by 20 dB and digitized by an oscilloscope (MSO54, Tektronix, Inc., Beaverton, OR, USA). Each signal is averaged by 8 times in the oscilloscope to promote stability.

D. Evaluation of Imaging Performance

The axial super-resolution performance of the quasi-monopolar pulse from the dual-frequency ultrasound transducer was evaluated experimentally with phantom wires [Fig. 3(a)]. Similar to that in the characterization, the generation of the quasi-monopolar pulse was realized by exciting both of the dual-frequency elements with specific combinations of time delay, frequency, and amplitude. Meanwhile, the oscilloscope receives the trigger signal from the function generator and digitizes the echo signals from the ultrasound transducer. A motion stage positions the transducer and realizes the mechanical scan to acquire a set of A-lines for synthetic aperture imaging. The whole system is under the control of LabVIEW (National Instruments Corporation, Austin, TX, USA), which synchronizes the dual-pulse excitation, the data acquisition, and the transducer positioning. The imaging target is a customized phantom with copper wires fixed between two acrylic plates. The diameter of each wire is 0.3 mm and the positions are indicated in Fig. 3(b).

Synthetic aperture and beamforming methods are used to reconstruct the ultrasound images. As the ultrasound scans the field of view mechanically, one waveform is acquired in each position. The synthetic aperture method combines the multiple waveforms acquired in the field of view and generates a dataset equivalent to an array signal. Subsequently, a minimum variance beam-former is used for the image reconstruction. The signal from each channel is specifically weighted before summing, which maximizes the energy output of the desired direction [41], [42].

For a demonstration of the high-definition imaging capability, the traditional imaging method with the individual 1 and 3 MHz ultrasound elements is included as the reference. Identical beamforming methods are used in all the single-frequency signals and the quasi-monopolar pulses. In traditional imaging, the peaks of the waveforms are not significantly larger than the residual waveforms; therefore, the envelopes of the beamformed echo signals are converted to B-mode images to avoid multiple peaks from one target. For the quasi-monopolar pulses, contrarily, there are no other residual waveforms according to Fig. 1(c), and the monopolar

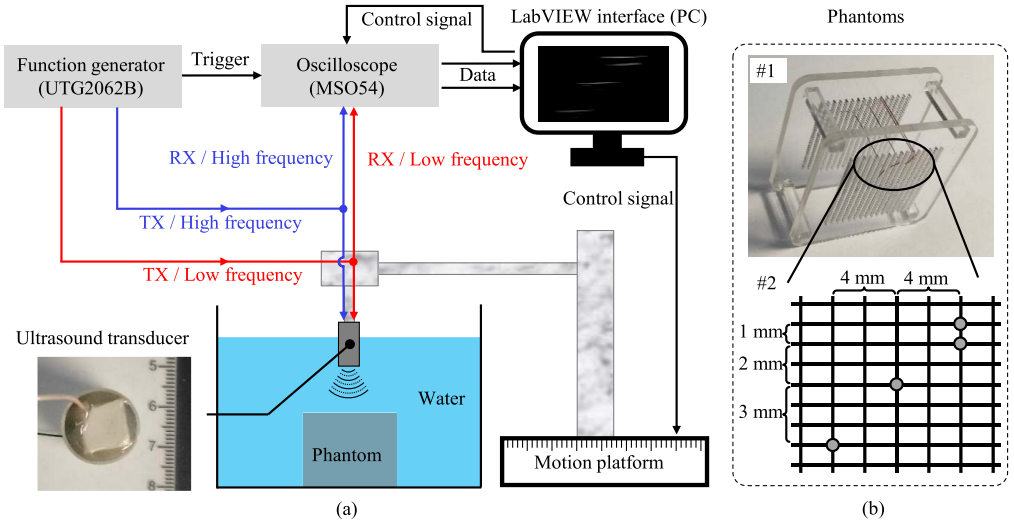

Fig. 3. (a) Overview diagram of the experimental setup, a photograph of the ultrasound transducer is included in the overview. (b) #1—Photographs of the phantom for the imaging and #2—Schematic diagram of copper wire placement in phantom, the horizontal distance is 2 mm, and the minimum vertical distance is 1 mm.

waveform itself indicates the position of the target with a high definition. Consequently, the short pulse is converted to B-mode images directly.

Furthermore, the robustness of the short-pulse method is validated by making two adjacent targets even closer, i.e., within 1 mm. The scatterers are two 0.2 mm diameter tungsten wires placed in parallel. The distances between the two wires vary between 0.3 and 0.7 mm. Other experimental setups and data processing methods are the same as described in this section.

III. Results and Discussion

A. Theoretical and Simulated Evaluation of the Pulses

The performance of the quasi-monopolar is evaluated theoretically to find out the optimal frequency and amplitude combinations between the two wavelets. As described above, the frequency ratio is in the range of 2–4.5, while the amplitude ratio is in the range of 0.5–3.5. The fractional bandwidth of each wavelet remains 70% in accordance with actual transducers. We evaluated the ratio between the peak pressure and the residual pressure (η) quantitatively. The single maximum value of η is 3.2, which shows up at a frequency ratio of 3.1 and an amplitude ratio of 2.1 [Fig. 4(a)]. This is the optimal combination for a dual-frequency ultrasound transducer with 70% bandwidth. Meanwhile, the gradient around the maximum value is low, and all the combinations inside the area of the dash lines result in an η of at least 2.88 (90% of the maximum value of η). This indicates the robustness of the method, and a slight deviation of the frequency or amplitude ratio does not degrade the quasi-monopolar pulses obviously.

A few representative points are selected in Fig. 4(a), the waveforms of which are calculated theoretically and simulated with FEM. With the given frequency and amplitude ratio, waveforms and the pressure output demonstrate the quasi-monopolar pulses. Point ① represents the optimal frequency and amplitude ratios with the highest η value. Point ② located on the dash line with suboptimal frequency and amplitude ratios, which generated an η value of 90% of the maximum. Points ③ and ④ correspond to other frequency and amplitude ratios with relatively low η value. All the calculated waveforms are symmetry referring to the peak value [Fig. 4(b)]. In comparison, the simulated waveforms are slightly asymmetry because there is an aliasing echo [38], [43] for the high-frequency component [Fig. 4(c)]. The aliasing echoes degrade the signals slightly, especially in the cases with relatively high η values (points ① and ②). Apart from the asymmetry, the FEM results match well with the calculation results [Fig. 4(b) versus (c)].

The fractional bandwidth and number of cycles in each wavelet are still dominant for the final performance of the quasi-monopolar pulses. For wavelets with a fractional bandwidth of 90%, generally the upper limit for transducers with piezoelectric 1–3 composite materials, the maximum value of η reaches 5.0 [Fig. 4(d) and (e)], which is very close to the monopolar waveform. The maximum value shows up at a frequency ratio of 3.1 and an amplitude ratio of 1.9, which is close to the case with 70% bandwidth. Moreover, the favorable areas [dashed line in Fig. 4(a) and (d)] are similar for both cases. (Both are 90% of the maximum value of η.) This indicates that the optimal ratios of frequency and amplitude are generally 3:1 and 2:1, respectively, which is relatively independent of the bandwidth of each wavelet. Considering the performance of other types of transducers, e.g., CMUT or PMUT, a broader bandwidth leads to a higher η value [Fig. 4(f)]. Waveforms for these cases are simulated with FEM because the bandwidth is not achievable by the dual-frequency transducer demonstrated in Fig. 2.

B. Characterization of Acoustic Pulses

The quasi-monopolar acoustic pulses are characterized experimentally by evaluating the pressure ratio η. The two

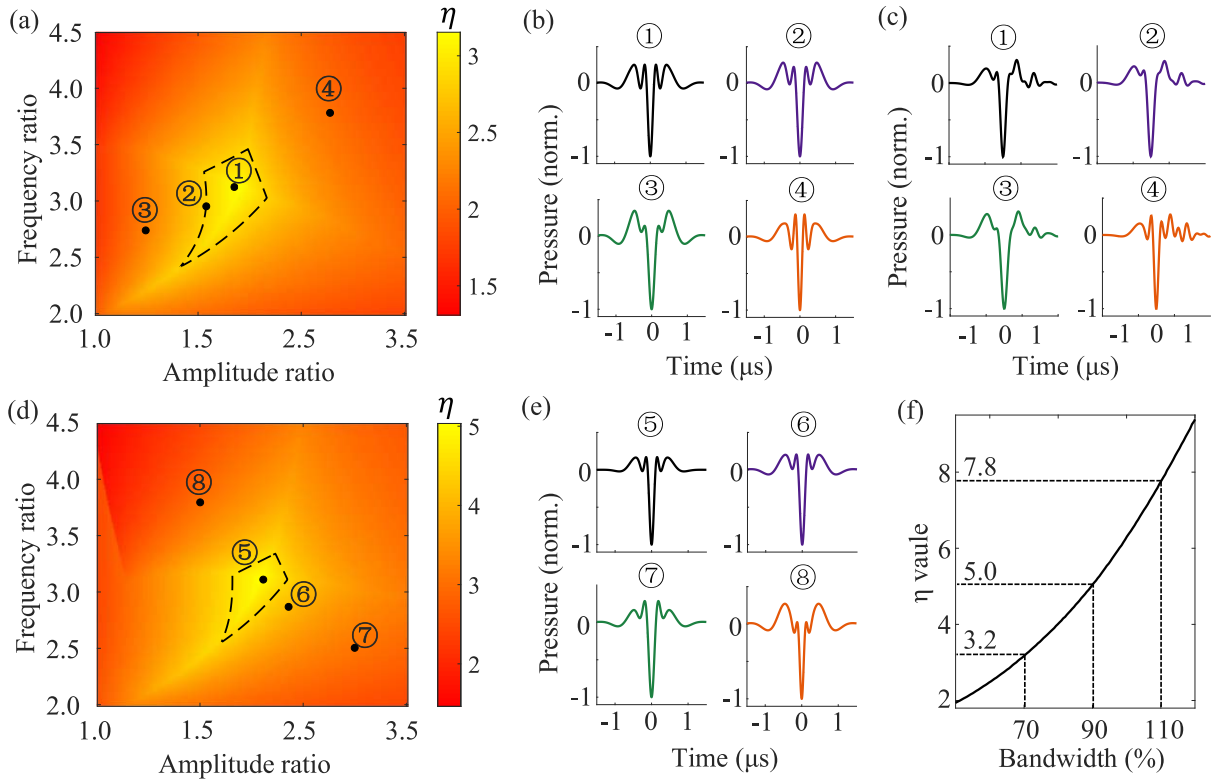

Fig. 4. η values and the waveforms dependent on the amplitude and frequency ratios. (a) and (d) η value maps with a fractional -6 dB bandwidth of 70% and 90%, respectively, for each wavelet. The dashed line indicates an η value of 90% relative to each peak. (b) and (c) Waveforms of theoretical and FEM simulations for Points ①–④ in (a), respectively. (e) Theoretical waveforms of Points ⑤–⑧ in (d). (f) Curve of maximum η values versus the bandwidth of each wavelet.

elements of the dual-frequency transducer were connected to the dual-channel function generator and excited individually. The excitation amplitude and frequency of the 1 MHz element remain at 5 V_{PP} and 1 MHz, respectively. The excitation amplitude and frequency of the 3 MHz elements vary according to the calculation results in Fig. 4(a). The center combination of the amplitude and frequency ratios is 2:1 and 3:1, respectively. The amplitude ratio ranges from 0.5 to 3.5 with an interval of 0.5. The frequency ratio ranges from 2 to 4.5 with a roughly geometric progression of 2, 2.45, 3, 3.6, and 4.5. To maintain the specific amplitude ratios for each configuration, the excitation voltage ranges for the high-frequency element are 1.32–9.21, 0.96–6.73, 0.86–6.03, 0.83–5.83, and 0.93–6.48 V_{PP}, respectively, corresponding to the frequency ratio of 2, 2.45, 3, 3, 6, and 4.5.

The experimental results demonstrated good agreement with the calculation results (Fig. 5). The maximum value of the pressure ratio η corresponds to the amplitude ratio of 2:1 and frequency ratio of 3:1. The value of η decreases gradually as the amplitude and frequency ratios deviate from the optimal one. The η values along the diagonal from the top-right to bottom-left are generally large compared to the top-left and bottom-right corners. Nevertheless, all the experimentally measured η values in Fig. 5(a) are slightly lower than those in Fig. 4(a). This originates from the fact that the performances of the dual-frequency elements in the fabricated transducer are not as ideal as the wavelets used in the calculation. First, the bandwidths of both elements are slightly narrower than that used in the calculation [Fig. 5(b)], which is the primary cause of the decreased η values. Furthermore, the reverberations between the two elements lead to an aliasing echo following the main pulses, which breaks the symmetry and increases the denominator in the calculation of η values. Moreover, the aliasing echo is the main reason for the residual pressure of 0.341, which decreases the η values further and deviates from the overall map of the η values.

The sound pressure signal waveform emitted by the transducer is close to the monopolar impulse response [Fig. 5(b)]. The η value reaches 2.94, indicating that the amplitude of the peak pulse is almost three times the peak-to-peak amplitude of the residual waveforms. The actual full-width at half-maximum (FWHM) pulse length (not the envelope) is only 150 ns, corresponding to 0.15 period and 0.45 period for the 1 and 3 MHz ultrasonic waves, respectively. The sub-wavelength quasi-monopolar waveform is far beyond the capability of traditional single-frequency ultrasound transducers. The -6 dB bandwidth of the sound pressure amplitude spectrum almost covers from 0.55 to 2.51 MHz with a slight gap at around 2 MHz, indicating a relative fractional bandwidth of almost 128.1%. The measured spectrum highly resembles the designed spectrum in Fig. 1(b). Here, the waveform is optimized by the maximum η value, which is non-optimal

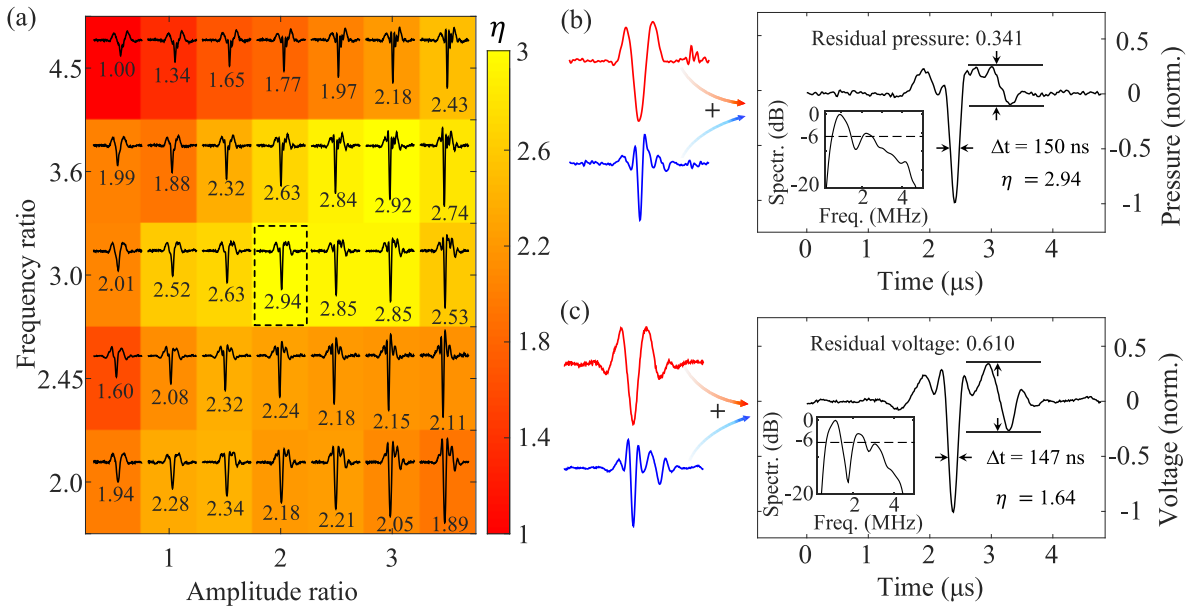

Fig. 5. (a) Measured signals with the given combinations of frequency and amplitude ratios. (b) Transmitted sound pressure at two frequencies and the quasi-monopolar pulse from the superposition of them. Inset: Spectrum of the sound pressure. (c) Pulse-echo voltage at two frequencies and the quasi-monopolar pulse from the superposition of them. Inset: Spectrum of the echo voltage.

for spectral coverage. Other combinations of frequency and amplitude ratio between the two sub-waveforms may lead to a broader bandwidth, which is beyond the topic in this research.

The pulse-echo response of the dual-frequency transducer is a voltage amplitude signal, which leads to a quasi-monopolar pulse by superposition of the two waveforms at two frequencies [Fig. 5(c)]. The pulse-echo signal is more adversely affected by the aliasing echo, which results in a residual amplitude of 0.610. Due to the twice convolution of the pulse-echo signal, the spectrum of the echo voltage demonstrates a narrower bandwidth and larger gap at 2 MHz compared with the transmission signal. Although the η value drops 1.64 for the optimal combination (with an amplitude ratio of 2:1 and a frequency ratio of 3:1), the FWHM pulse length remains the same as 0.15 and 0.45 period for the 1 and 3 MHz ultrasonic waves, respectively. This sub-wavelength quasi-monopolar pulse indicates the potential of discernibility for ultra-fine structures in the axial direction. The residual waveforms around the main pulse do not decrease the axial resolution. However, the SNR would decrease because the residual waveforms are noises in the imaging. Increasing the bandwidth and decreasing the pulse length of the dual-frequency transducer is an effective way of suppressing the residual waveforms, which is also the key to all piezoelectric ultrasound transducers.

C. Imaging of Phantoms

Experimental imaging with the quasi-monopolar pulses validates the capability of the dual-frequency transducer for resolving fine structures. Synthetic aperture and beamforming methods have been used for the signal from each frequency. For reference, we used each signal to generate a B-mode image individually [Fig. 6(a) and (b)]. For the super-resolution imaging, the two signals were super-positioned to generate the quasi-monopolar pulses and to reconstruct the axial super-resolution image [Fig. 6(c)]. Compared with the images from the 1 or 3 MHz ultrasound waves, the quasi-monopolar signal generated a significantly high-definition image (Fig. 6). The 1 MHz signal is similar to a Gaussian waveform, therefore, the point spread function is relatively uniform with only one peak along the axial direction [Fig. 6(a)]. The FWHM pulse length is 1.33 mm (converted to spatial domain), which is normal for a 1 MHz ultrasound wave. It is impossible to differentiate the two phantom wires with a 1 mm distance. The 3 MHz ultrasound signal exhibits a short FWHM pulse length of 0.31 mm [Fig. 6(b)]. Nevertheless, the aliasing echoes following the main pulses are noises in the image, which makes it impossible to differentiate the two phantom wires with a 1 mm distance either. Contrarily, the FWHM pulse length of the quasi-monopolar pulse is only 0.08 mm without other noises [Fig. 6(c)], which is only 0.11λ for a waveform at 2 MHz center frequency. With this ultra-short pulse length, the signal distinguishes all four phantom wires with high definition.

The quasi-monopolar pulses promote the axial resolution but not the lateral resolution, which agrees well with the theory. The axial resolution is directly determined by the pulse length, whereas the lateral resolution is determined by the beam width. In this experiment, the two elements in the dual-frequency transducer work together to generate a short pulse, which is equivalent to a single-element transducer. The bandwidth of the transducer is wide, yielding a wide point spread function and low resolution in the lateral direction. Consequently, the lateral resolutions for either single-frequency imaging or quasi-monopolar imaging are all low. This problem would be

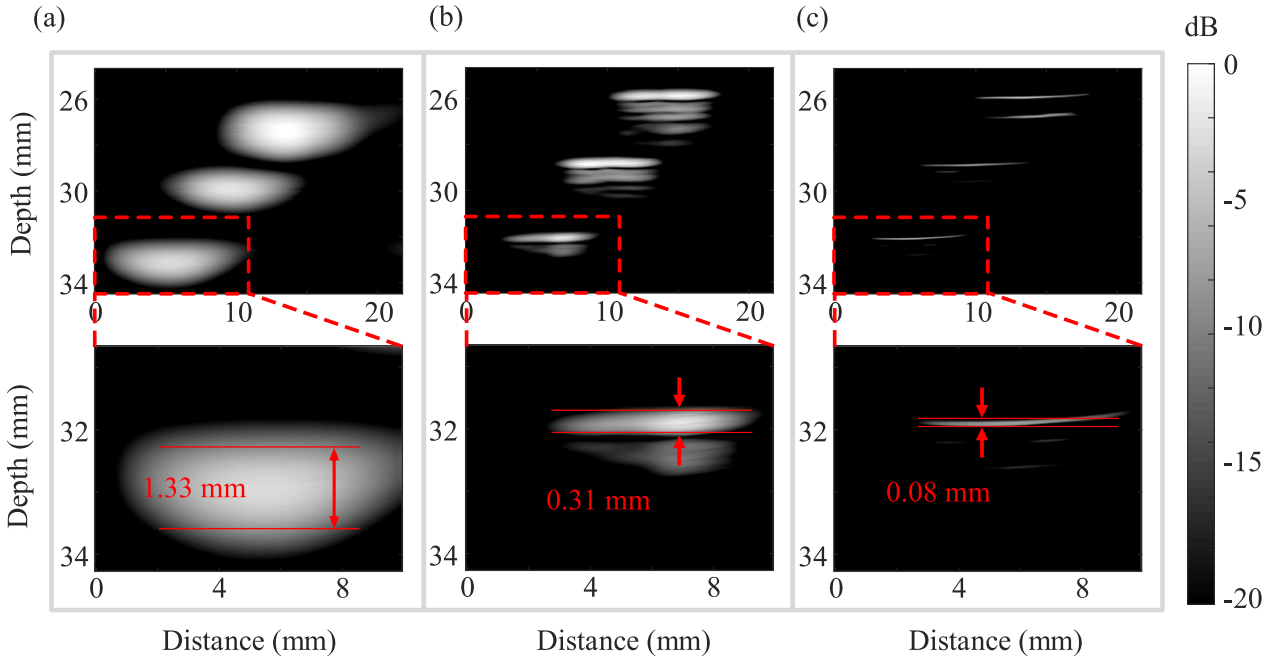

Fig. 6. B-mode image of single frequency signal and superposition signal. (a) and (b) B-mode images of 1 and 3 MHz signals. (c) B-mode image of superposition signal.

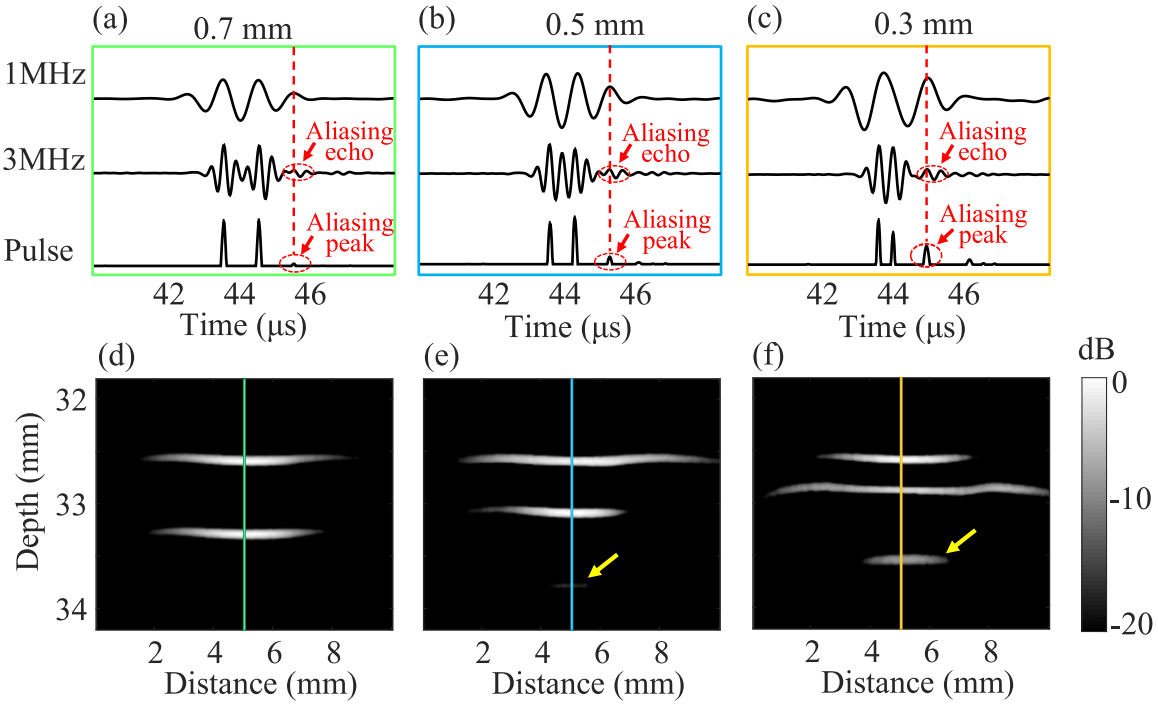

Fig. 7. Imaging performance as the two scatterers getting close to each other. (a)–(c) Echo waveforms at each frequency and the processed quasi-monopolar pulses. (d)–(f) B-mode images generated from the signals above. The distance between the two scatterers are 0.7, 0.5, and 0.3 mm as indicated on top of (a) and (d), (b) and (e), and (c) and (f), respectively.

solved by upgrading the dual-frequency transducer to a dual-frequency array. Beamforming and image reconstruction from the array would promote the lateral resolution significantly.

As the distance between two scatterers getting closer, additional aliasing peaks would show up (Fig. 7). At a distance of 0.7 mm (0.93λ for a 2 MHz sound wave, shown in Fig. 7 (a) and (d), the aliasing peaks are almost invisible (–26 dB relative to peak amplitude), and the two scatters are clearly distinguishable without known drawbacks. As the distance getting closer to 0.5 mm (0.67λ, shown in Fig. 7 (b) and (e), an aliasing peak is barely visible (–16 dB), which is negligible in the imaging. If the distance is 0.3 mm (0.4λ, shown in Fig. 7

(c) and (f), the two scatterers are still clearly distinguishable. However, the maximum aliasing peak increases to –8 dB, which is clearly visible and unacceptable in most imaging cases. As mentioned above, the actual ultrasound signals in the study are asymmetry due to the aliasing echoes for the high-frequency ultrasound. These aliasing echoes result in the aliasing peaks in the quasi-monopolar pulses. Suppressing the aliasing echoes with acoustic filter layers [38] would help reducing the aliasing peaks in the pulses, which is expected to decrease the bandwidth of the high-frequency pulses though.

IV. Conclusion

This study illustrated the feasibility of generating quasi-monopolar ultrasound pulses by the stack-layer dual-frequency ultrasound transducer for super-resolution imaging in the axial direction. The quasi-monopolar pulses generated by the dual-frequency transducer overcome the limit of traditional ultrasound transducers, providing an effective way to shorten the pulses and broaden the bandwidth. The proposed imaging method with the quasi-monopolar pulses results in superb resolving capability with high definition in the axial direction. Two scatterers with a distance of 0.67λ are clearly resolvable with barely visible additional noises. This indicates a super-resolution approach for general-purpose imaging without special markers or contrast agents. For scatterers with even closer distance (e.g., 0.4λ), the scatterers are still clearly distinguishable, which is beyond the capability of traditional ultrasound imaging. Nevertheless, aliasing peaks show up gradually, which degrades the overall imaging quality. In conclusion, this work proposes a method to generate quasi-monopolar pulses by stack-layer dual-frequency ultrasound transducers, and demonstrated super-resolution imaging capability in the axial direction.

References

[1] E. Betzig et al., "Imaging intracellular fluorescent proteins at nanometer resolution," *Science*, vol. 313, no. 5793, pp. 1642–1645, Sep. 2006.

[2] C. Kupsch, L. Feierabend, R. Nauber, L. Buttner, and J. Czarske, "Ultrasound super-resolution flow measurement of suspensions in narrow channels," *IEEE Trans. Ultrason., Ferroelectr., Freq. Control*, vol. 68, no. 3, pp. 807–817, Mar. 2021.

[3] H. Liang, X. Wu, J. Xue, and K. Lu, "Thickness measurement of graphite coating on lithium battery anode film by scanning acoustic microscope with resolution enhancement method," *IEEE Trans. Instrum. Meas.*, vol. 71, pp. 1–12, 2022.

[4] Z. Jiang, R. J. Dickinson, T. L. Hall, and J. J. Choi, "A PZT–PVDF stacked transducer for short-pulse ultrasound therapy and monitoring," *IEEE Trans. Ultrason., Ferroelectr., Freq. Control*, vol. 68, no. 6, pp. 2164–2171, Jun. 2021.

[5] Z. Zhang et al., "Design and comparison of PMN-PT single crystals and PZT ceramics based medical phased array ultrasonic transducer," *Sens. Actuator A, Phys.*, vol. 283, pp. 273–281, Nov. 2018.

[6] X. Ma, M. Fan, Y. Cai, L. Xu, and J. Ma, "A Fabry–Pérot fiber-optic array for photoacoustic imaging," *IEEE Trans. Instrum. Meas.*, vol. 71, pp. 1–8, 2022.

[7] C. Errico et al., "Ultrafast ultrasound localization microscopy for deep super-resolution vascular imaging," *Nature*, vol. 527, no. 7579, pp. 499–502, Nov. 2015.

[8] J. Cowe, J. Gittins, and D. H. Evans, "Coded excitation in TCD ultrasound systems to improve axial resolution," *Ultrasound Med. Biol.*, vol. 33, no. 8, pp. 1296–1308, Aug. 2007.

[9] J.-H. Sung and J.-H. Chang, "Mechanically rotating intravascular ultrasound (IVUS) transducer: A review," *Sensors*, vol. 21, no. 11, p. 3907, Jun. 2021.

[10] M. Almualimi, M.-L. Wille, and C. M. Langton, "Potential for ultrasound transit time spectroscopy to improve axial resolution," *Appl. Acoust.*, vol. 133, pp. 91–96, Apr. 2018.

[11] C. Peng, H. Wu, S. Kim, X. Dai, and X. Jiang, "Recent advances in transducers for intravascular ultrasound (IVUS) imaging," *Sensors*, vol. 21, no. 10, p. 3540, May 2021.

[12] N. Wang et al., "An improved chirp coded excitation based on compression pulse weighting method in endoscopic ultrasound imaging," *IEEE Trans. Ultrason., Ferroelectr., Freq. Control*, vol. 68, no. 3, pp. 446–452, Mar. 2021.

[13] J. Lee and J. H. Chang, "Dual-element intravascular ultrasound transducer for tissue harmonic imaging and frequency compounding: Development and imaging performance assessment," *IEEE Trans. Biomed. Eng.*, vol. 66, no. 11, pp. 3146–3155, Nov. 2019.

[14] X. Ma and W. Cao, "Single-crystal high-frequency intravascular ultrasound transducer with 40-μm axial resolution," *IEEE Trans. Ultrason., Ferroelectr., Freq. Control*, vol. 67, no. 4, pp. 810–816, Apr. 2020.

[15] M. Su et al., "Cable-shared dual-frequency catheter for intravascular ultrasound," *IEEE Trans. Ultrason., Ferroelectr., Freq. Control*, vol. 66, no. 5, pp. 849–856, May 2019.

[16] L. Peralta, A. Ramalli, M. Reinwald, R. J. Eckersley, and J. V. Hajnal, "Impact of aperture, depth, and acoustic clutter on the performance of coherent multi-transducer ultrasound imaging," *Appl. Sci.*, vol. 10, no. 21, p. 7655, Oct. 2020.

[17] R. P. Zangabad et al., "Real-time coded excitation imaging using a CMUT-based side looking array for intravascular ultrasound," *IEEE Trans. Ultrason., Ferroelectr., Freq. Control*, vol. 68, no. 6, pp. 2048–2058, Jun. 2021.

[18] D. Dalecki, S. Z. Child, C. H. Raeman, C. Xing, S. Gracewski, and E. L. Carstensen, "Bioeffects of positive and negative acoustic pressures in mice infused with microbubbles," *Ultrasound Med. Biol.*, vol. 26, no. 8, pp. 1327–1332, Oct. 2000.

[19] M. B. Butler, D. H. Thomas, N. Silva, S. D. Pye, and V. Sboros, "On the acoustic response of microbubbles in arteriole sized vessels," *Appl. Phys. Lett.*, vol. 99, no. 19, Nov. 2011, Art. no. 193702.

[20] A. Trucco and F. Bertora, "Harmonic beamforming: Performance analysis and imaging results," *IEEE Trans. Instrum. Meas.*, vol. 55, no. 6, pp. 1965–1974, Dec. 2006.

[21] H. Fang, Z. Qiu, A. J. Mulholland, R. L. O'Leary, and A. Gachagan, "Broadband 1–3 piezoelectric composite transducer design using Sierpinski gasket fractal geometry," *IEEE Trans. Ultrason., Ferroelectr., Freq. Control*, vol. 65, no. 12, pp. 2429–2439, Dec. 2018.

[22] D. Liu et al., "Broadband and high sensitive time-of-flight diffraction ultrasonic transducers based on PMNT/epoxy 1–3 piezoelectric composite," *Sensors*, vol. 15, no. 3, pp. 6807–6817, Mar. 2015.

[23] K. Song, J.-H. Kwak, J. J. Park, and S. Hur, "Acoustic metasurfaces for efficient matching of non-contact ultrasonic transducers," *Smart Mater. Struct.*, vol. 30, no. 8, Aug. 2021, Art. no. 085011.

[24] X. Sun et al., "Intelligent optimization of matching layers for piezoelectric ultrasonic transducer," *IEEE Sensors J.*, vol. 21, no. 12, pp. 13107–13115, Jun. 2021.

[25] X. Yang et al., "Multi-layer polymer-metal structures for acoustic impedance matching in high-frequency broadband ultrasonic transducers design," *Appl. Acoust.*, vol. 160, Mar. 2020, Art. no. 107123.

[26] B. Jadidian, N. M. Hagh, A. A. Winder, and A. Safari, "25 MHz ultrasonic transducers with lead-free piezoceramic, 1–3 PZT fiber-epoxy composite, and PVDF polymer active elements," *IEEE Trans. Ultrason., Ferroelectr., Freq. Control*, vol. 56, no. 2, pp. 368–378, Feb. 2009.

[27] K.-B. Kim, D. K. Hsu, B. Ahn, Y.-G. Kim, and D. J. Barnard, "Fabrication and comparison of PMN-PT single crystal, PZT and PZT-based 1–3 composite ultrasonic transducers for NDE applications," *Ultrasonics*, vol. 50, no. 8, pp. 790–797, Aug. 2010.

[28] A. S. Savoia, G. Caliano, and M. Pappalardo, "A CMUT probe for medical ultrasonography: From microfabrication to system integration," *IEEE Trans. Ultrason., Ferroelectr., Freq. Control*, vol. 59, no. 6, pp. 1127–1138, Jun. 2012.

[29] Z. Zheng et al., "Development of a novel CMUT-based concentric dual-element ultrasonic transducer: Design, fabrication, and characterization," *J. Microelectromech. Syst.*, vol. 27, no. 3, pp. 538–546, Jun. 2018.

[30] M. Maadi, C. Ceroici, and R. J. Zemp, "Dual-frequency CMUT arrays for multiband ultrasound imaging applications," *IEEE Trans. Ultrason., Ferroelectr., Freq. Control*, vol. 68, no. 7, pp. 2532–2542, Jul. 2021.

[31] S. Sadeghpour, S. V. Joshi, C. Wang, and M. Kraft, "Novel phased array piezoelectric micromachined ultrasound transducers (pMUTs) for medical imaging," *IEEE Open J. Ultrason., Ferroelectr., Freq. Control*, vol. 2, pp. 194–202, 2022.

[32] W. Zhu, L. Wang, Z. Wu, W. Liu, and C. Sun, "Broadband piezoelectric micromachined ultrasonic transducer with a resonant cavity," *IEEE Trans. Ultrason., Ferroelectr., Freq. Control*, vol. 69, no. 1, pp. 340–349, Jan. 2022.
[33] S. Liao, L. Ou, and L. Xu, "Super-resolution ultrasound Lamb wave NDE imaging of anisotropic airplane laminates via deconvolutional neural network," *IEEE Trans. Instrum. Meas.*, vol. 70, pp. 1–8, 2021.
[34] L. Svilainis, A. Rodriguez-Martinez, A. Chaziachmetovas, and A. Aleksandrovas, "Ultrasound transmission spectral compensation using arbitrary position and width pulse sets," *IEEE Trans. Instrum. Meas.*, vol. 67, no. 8, pp. 1778–1785, Aug. 2018.
[35] K.-W. Lin, T. L. Hall, R. J. McGough, Z. Xu, and C. A. Cain, "Synthesis of monopolar ultrasound pulses for therapy: The frequency-compounding transducer," *IEEE Trans. Ultrason., Ferroelectr., Freq. Control*, vol. 61, no. 7, pp. 1123–1136, Jul. 2014.
[36] Y. Cai, S. Song, L. Xu, and J. Ma, "Quasi-monopolar ultrasound pulse by stack-layer dual-frequency ultrasound transducer," in *Proc. IEEE Int. Ultrason. Symp. (IUS)*, Sep. 2021, pp. 1–3.
[37] X. Luo et al., "Stack-layer dual-element ultrasonic transducer for broadband functional photoacoustic tomography," *Frontiers Bioeng. Biotechnol.*, vol. 9, Oct. 2021, Art. no. 786376.
[38] J. Ma, M. B. Steer, and X. Jiang, "An acoustic filter based on layered structure," *Appl. Phys. Lett.*, vol. 106, no. 11, Mar. 2015, Art. no. 111903.
[39] X. Deng et al., "Design and fabrication of a novel dual-frequency confocal ultrasound transducer for microvessels super-harmonic imaging," *IEEE Trans. Ultrason., Ferroelectr., Freq. Control*, vol. 68, no. 4, pp. 1272–1277, Apr. 2021.
[40] X. Sun, X. Yang, X. Zhu, and H. Liu, "Dual-frequency ultrasound transducers for the detection of morphological changes of deep-layered muscles," *IEEE Sensors J.*, vol. 18, no. 4, pp. 1373–1383, Feb. 2018.
[41] J. Capon, "High-resolution frequency-wavenumber spectrum analysis," *Proc. IEEE*, vol. 57, no. 8, pp. 1408–1418, Aug. 1969.
[42] Z. Lan, C. Zheng, Y. Wang, H. Peng, and H. Qiao, "Adaptive threshold for eigenspace-based minimum variance beamformer for dark region artifacts elimination," *IEEE Trans. Instrum. Meas.*, vol. 70, pp. 1–16, 2021.
[43] J. Ma et al., "Design factors of intravascular dual frequency transducers for super-harmonic contrast imaging and acoustic angiography," *Phys. Med. Biol.*, vol. 60, no. 9, pp. 3441–3457, May 2015.

Yiqi Cai received the B.S. degree from Tianjin University, Tianjin, China, in June 2017.

In September 2018, he joined the School of Instrumentation and Optoelectronics Engineering, Beihang University, Beijing, China, as a Ph.D. Student, supervised by Jianguo Ma. His current research interests include the design of novel ultrasound transducers and the study of super-resolution ultrasound imaging algorithms.

Mengzhi Fan received the B.S. degree from Sichuan University, Chengdu, China, in June 2019.

In September 2019, she joined the School of Instrumentation and Optoelectronics Engineering, Beihang University, Beijing, China, as a Ph.D. Student, supervised by Jianguo Ma. Her current research interests include medical ultrasound imaging, especially imaging methods based on novel ultrasound sensors.

Pengfei Sun is currently a Radiologist with the Department of Ultrasound, Beijing Friendship Hospital, Capital Medical University, Beijing, China. Her current research interests include ultrasound diagnosis and interventional therapy.

Lijun Xu (Fellow, IEEE) received the Ph.D. degree in electrical engineering and instrumentation from Tianjin University, Tianjin, China, in 1996.

From 1997 to 2001, he was an Associate Professor with the School of Electrical Engineering and Automation, Tianjin University. From January 2002 to 2006, he was a Research Fellow and a Higher Scientific Officer with the University of Greenwich, London, U.K.; the University of Kent, Canterbury, U.K.; and the Institute of Cancer Research, University of London, London. He is currently a Professor and the Dean of the School of Instrument Science and Opto-Electronic Engineering, Beihang University, Beijing, China. His current research interests include tomographic imaging, digital imaging, and dynamic process monitoring.

Jianguo Ma (Member, IEEE) received the B.S. and M.S. from Shandong University, Jinan, China, in 2008 and 2011, respectively, and the Ph.D. degree from North Carolina State University, Raleigh, NC, USA, in 2014.

He was a Research Scientist with the University of California, Los Angeles, CA, USA, from 2015 to 2016. He has been an Associate Professor with Beihang University, Beijing, China, since 2016. His current research interests include medical ultrasound imaging, piezoelectric ultrasound transducers, optical ultrasound sensing, and quantitative ultrasound for smart diagnosis.